Translational Oncology
www.transonc.com

Volume 6 Number 3 June 2013 pp. 234–243 234

Conventional Frequency Ultrasonic Biomarkers of Cancer Treatment Response *In Vivo*[1,2]

Ali Sadeghi-Naini*,†,‡,§, Omar Falou*,†,‡,§, Hadi Tadayyon*,‡, Azza Al-Mahrouki*,†, William Tran†, Naum Papanicolau*, Michael C. Kolios‡,¶ and Gregory J. Czarnota*,†,‡,§,¶

*Imaging Research - Physical Sciences, Sunnybrook Research Institute, Sunnybrook Health Sciences Centre, Toronto, Ontario, Canada; †Department of Radiation Oncology, Odette Cancer Centre, Sunnybrook Health Sciences Centre, Toronto, Ontario, Canada; ‡Department of Medical Biophysics, Faculty of Medicine, University of Toronto, Toronto, Ontario, Canada; §Department of Radiation Oncology, Faculty of Medicine, University of Toronto, Toronto, Ontario, Canada; ¶Department of Physics, Ryerson University, Toronto, Ontario, Canada

Abstract

BACKGROUND: Conventional frequency quantitative ultrasound in conjunction with textural analysis techniques was investigated to monitor noninvasively the effects of cancer therapies in an *in vivo* preclinical model. *METHODS:* Conventional low-frequency (~7 MHz) and high-frequency (~20 MHz) ultrasound was used with spectral analysis, coupled with textural analysis on spectral parametric maps, obtained from xenograft tumor–bearing animals (n = 20) treated with chemotherapy to extract noninvasive biomarkers of treatment response. *RESULTS:* Results indicated statistically significant differences in quantitative ultrasound-based biomarkers in both low- and high-frequency ranges between untreated and treated tumors 12 to 24 hours after treatment. Results of regression analysis indicated a high level of correlation between quantitative ultrasound-based biomarkers and tumor cell death estimates from histologic analysis. Applying textural characterization to the spectral parametric maps resulted in an even stronger correlation (r^2 = 0.97). *CONCLUSION:* The results obtained in this research demonstrate that quantitative ultrasound at a clinically relevant frequency can monitor tissue changes *in vivo* in response to cancer treatment administration. Using higher order textural information extracted from quantitative ultrasound spectral parametric maps provides more information at a high sensitivity related to tumor cell death.

Translational Oncology (2013) 6, 234–243

Introduction

Cancer patients respond differently to identical treatments. As such, a predefined therapy is not often effective for all patients. This makes the early detection of patients refractory to a specific therapy critical, since this could facilitate a switch to an early salvage therapy or a change to a more effective primary treatment [1]. For example, locally advance breast cancer patients can considerably benefit from an early evaluation of their ultimate response to the neoadjuvant chemotherapy, as an important component of their therapy, since a complete pathologic response to neoadjuvant chemotherapy has been demonstrated to have a strong correlation with patient survival [2–4]. However, this

Address all correspondence to: Dr Gregory J. Czarnota, Department of Radiation Oncology and Physical Sciences, Sunnybrook Health Sciences Centre, 2075 Bayview Avenue, T2-167, Toronto, Ontario M4N 3M5, Canada. E-mail: Gregory.Czarnota@sunnybrook.ca

[1]A.S.N. and O.F. hold a Canadian Breast Cancer Foundation Postdoctoral Fellowship. H.T. holds a Natural Sciences and Engineering Research Council of Canada Alexander Graham Bell Graduate Scholarship. G.J.C. holds a Cancer Care Ontario Research Chair in experimental therapeutics and imaging. This study was funded, in part, by the Canadian Breast Cancer Foundation, Ontario Region. Funding for this project was also provided by the Terry Fox Foundation and the Natural Sciences and Engineering Research Council of Canada.

[2]This article refers to supplementary material, which is designated by Figure W1 and is available online at www.transonc.com.

Received 7 November 2012; Revised 11 February 2013; Accepted 14 February 2013

DOI 10.1593/tlo.12385

prognostic factor is frequently assessed at the time of surgery, and at this time, the window for modifying neoadjuvant treatment is already passed. Standard anatomic-based imaging can detect macroscopic changes in tumor size as a measure of treatment response. However, such changes often take many weeks to months to develop, and in some cases, abnormal tissue diminishment is not detectable even with a positive treatment response [5]. Functional imaging, including magnetic resonance imaging, diffuse optical imaging, and positron emission tomography, has been demonstrated as a method capable of detecting tumor responses after starting therapy [5–7]. Such methods that measure tumor physiology noninvasively could be used to facilitate changes in treatment to improve the patient's prognosis. In this context, quantitative ultrasound techniques have been recently demonstrated to be able to quantify changes in tissue microstructures that can be linked to effects of cancer therapies including apoptotic cell death. This has been demonstrated through several *in vitro*, *in situ*, and *in vivo* studies using high-frequency quantitative ultrasound techniques [8–15]. Ultrasound imaging is a high-resolution portable imaging modality with low cost and rapid imaging speed. In addition, unlike other modalities proposed for therapy response monitoring, it does not require injection of any contrast agents. This is principally due to the fact that alterations in the physical properties of dying cancer cells are the main source of the changes in image contrast and spectral features associated with tumor response [8].

Quantitative ultrasound techniques have been used in several tissue characterization applications where they have demonstrated capabilities for differentiating between tissues with different intrinsic microstructures. Such applications include the diagnosis of cardiac and liver abnormalities, prostate cancer, and the differentiation of benign from malignant diseases [16–18]. Specifically, with respect to breast cancer applications, Oelze et al. used quantitative ultrasound to differentiate fibroadenomas from mammary carcinomas and sarcomas [19].

Initial investigations for detecting apoptosis using quantitative ultrasound were performed using high-frequency (20–50 MHz) ultrasound with acute myeloid leukemia cell samples *in vitro* exposed to the chemotherapeutic agent cisplatin. Large increases obtained in the ultrasound backscatter amplitude demonstrated an increased tissue echogenicity 24 hours after drug exposure that were associated with cell death [8,9]. In subsequent studies, cellular nuclear structure was further linked to ultrasound backscatter properties in an examination of different cell types and their isolated nuclei in which speed of sound, attenuation coefficient, and integrated backscatter coefficient were measured [15]. The findings suggested that integrated backscatter coefficient values, but not attenuation or speed of sound, were correlated with the size of the nuclei. Further experiments conducted on mixtures of apoptotic cells and viable cells using high-frequency quantitative ultrasound indicated further increases in backscattered signal intensity compared to pure populations of apoptotic cells, indicating a role for effects of scatterer positions and their potential randomization in contributing to increases associated with cell death *in vivo* [11]. High-frequency quantitative ultrasound techniques have also been applied successfully in the detection of effects of photodynamic therapy and radiation therapy in other studies [12–14]. Those studies demonstrated that high-frequency ultrasound is sensitive to structural changes associated with cell death with considerable increases in ultrasound-based measures, such as backscattered signal intensity, which were accompanied by changes in spectral slope and 0-MHz intercept biomarkers (defined later).

One major limitation for the clinical application of high-frequency ultrasound is the limited depth of its penetration that constrains its use to superficial tissues. Conventional frequency (1–20 MHz) ultrasound, which is broadly used in medicine, benefits from a deeper tissue penetration but has a lower resolution (80 μm–1.5 mm). As such, conventional frequency ultrasound may potentially be able to evaluate patient responses to treatment for a variety of deeper sited cancers [20] such as liver [21–23], kidney [24–26], and breast [27–29] malignancies. The application of conventional frequencies to monitor morphologic alterations associated with cell death could accordingly permit evaluation of response to the cancer therapies and facilitate switching from ineffective treatments to more efficacious ones.

In this study, we investigate the potential of clinically relevant conventional frequency quantitative ultrasound to monitor noninvasively the effects of cancer therapies in an *in vivo* preclinical model. Assessments of xenograft tumor responses to cancer treatments were carried out using low-frequency (~7 MHz) ultrasound to demonstrate the feasibility of using conventional frequency quantitative ultrasound to detect and monitor cell death. Human breast cancer (MDA)–bearing mice were treated with intravenous paclitaxel-doxorubicin, and high- and low-frequency ultrasound data were acquired at different times after exposure. Ultrasound data analysis used linear regression analysis of the power spectrum, statistical analysis of the signal envelope, and novel texture analysis on spectral parametric maps as early biomarkers of treatment response to assess response heterogeneity. Results demonstrate the capacity of conventional frequency ultrasound integrated with textural analysis techniques in monitoring apoptotic tumor cell death resulting from cancer therapy administration. Statistically significant differences were revealed after 12 and 24 hours for both spectral and textural changes in midband fit (MBF) and 0-MHz intercept, respectively, as quantitative ultrasound-based biomarkers of treatment response. Regression analysis also revealed a strong correlation between changes in these ultrasonic biomarkers and the percentage of tumor cell death obtained from histologic analysis (r^2 = 0.97 for hybrid textural biomarkers). This research, thus, extends the applicability of quantitative ultrasound methods to clinical ranges of ultrasound for the detection of cell death *in vivo*.

Materials and Methods

Experimental Design and Data Collection

This study was conducted with research ethics approval from the Animal Care Committee of Sunnybrook Research Institute (Protocol No. 11-440). All animal handling was in accordance with the recommendations of the Canadian Council on Animal Care, requirements under the Animals for Research Act, RSO 1980, and institutional animal care committee policies and guidelines. Human breast cancer cells [MDA-MB-231; American Type Culture Collection (ATCC), Manassas, VA] were injected (1×10^6 cells) and permitted to grow to a size of 7- to 9-mm xenograft tumors in the hind leg of severe combined immunodeficiency disease (SCID) mice. Mice were anesthetized before imaging using 100 mg/kg ketamine, 5 mg/kg xylazine, and 1 mg/kg acepromazine (CDMV, St Hyacinthe, Quebec). Anesthetized animals were treated with paclitaxel-doxorubicin (150 mg/m^2, 50 mg/m^2, respectively) through intravenous tail vein injection. Experimentation used 20 animals (five groups of n = 4), one of which remained untreated as a control group. Each of the groups was assessed at a different time after chemotherapy exposure, i.e., 0, 4, 12, 24, and 48 hours, respectively, to determine the effect of treatment time on tumor response. Each mouse was imaged twice, i.e., before and after treatment. All

animals were killed following experiment, and tumors were excised for histologic examination.

Ultrasound radiofrequency (RF) data were collected using both conventional low- and high-frequency ultrasound. For low-frequency ultrasound, a Sonix RP System (Ultrasonix, Vancouver, British Columbia) was used with an L14-5/38 transducer with a transmit frequency of 10 MHz resulting in a bandwidth with a center frequency of ~7 MHz, focused at 1.5-cm depth, with data sampled at 40 MHz. High-frequency data were collected using a Vevo 770 System (Visual Sonics, Toronto, Ontario) using a transducer (RMV-710B) with a transmit frequency of 25 MHz resulting in a bandwidth with a center frequency of ~20 MHz, focused at 9-mm depth, with data sampled at 420 MHz. Both systems were used to collect three-dimensional data with scan plane separations of ~0.5 mm in the conventional frequency data and ~0.1 mm in the high-frequency data.

Ultrasound RF Data Analysis

Ultrasound RF data analysis was performed using the normalized power spectrum [8–10,12–14,17–19,30–32], and novel textural analysis on spectral parametric maps [27,33], to extract quantitative biomarkers of treatment response. Statistical analysis of the signal envelope [11,34] was also performed as an adjunct study.

Statistical tests of significance based on changes in determined parameters, compared to pretreatment data, were carried out using one-way analyses of variance (ANOVAs, $\alpha = 0.05$) over all treatment groups, for both conventional frequency and high-frequency data. Fisher's least significant difference (LSD) post hoc tests were then performed for each significant parameter to identify the treated groups with significant difference compared to the untreated control group.

Normalized spectral parameters. Ultrasound data were analyzed across 10 to 14 equally spaced scan planes with a size of 3.8 by 3.0 cm. Standardized regions of interest (ROIs), which were located at the tumor center, were used for analysis. Power spectra were calculated using a Fourier transform of the raw RF data for each scan line through the ROI and subsequently averaged. Data were normalized with a calibration pulse obtained from a flat quartz plate for high-frequency data [30]. Conventional frequency data normalization used the averaged power spectrum obtained from an agar-embedded glass-bead phantom model [35]. This was used for conventional frequency data, since it more accurately represented the frequency distribution obtained in tissue power spectrum data than that obtained from a quartz reflector at low frequencies. In addition, since conventional frequency ultrasound is eventually intended for clinical applications, phantom normalization can provide an approximate attenuation correction with depth, particularly for cases in which tumors are not superficial, e.g., in breast. Linear regression analysis was performed on the averaged power spectrum within a center frequency–based –6 dB window to generate a best-fit line. Parameters extracted include the MBF, the spectral slope, and the corresponding 0-MHz intercept [31,32,36,37].

Textural parameters. Spectral parametric maps were generated through a sliding window analysis within the ROI on a pixel-by-pixel basis, using a Hamming function. Maps were generated for MBF and 0-MHz intercept parameters as these parameters were relatively strongly correlated to tumor response on ROI-based average analysis. Texture analysis on parametric maps of MBF and 0-MHz intercept was performed on the basis of a gray-level co-occurrence matrix (GLCM), which represents the angular relationship between neighboring pixels as well as the distance between them [27,33]. Sixteen symmetric GLCMs were constructed considering each pixel's neighbors located at a distance of one to four pixels with angular values of 0° to 135° at 45° increments. Textural parameters (contrast, energy, and homogeneity) were extracted from the corresponding GLCMs of each spectral parametric map and were subsequently averaged [33].

Statistical parameters. Confirmatory statistical analysis of the signal envelope, another method to quantify ultrasound signals, was performed through measurements of the acquired signal's envelope histogram [38] by probability density function estimation [11]. Probability density function estimation of the envelope histogram was carried out by fitting a Rayleigh distribution that provided a suitable fit to both low- and high-frequency data [34].

Histologic Analysis

Histologic analysis was performed on tumor samples fixed in 5% formalin for 24 to 48 hours. Fixed tumor sections were cut in three representative planes with hematoxylin and eosin (H&E) staining carried out in addition to *in situ* end nick labeling (ISEL) immunohistochemistry for cell death. Microscopy was performed using a Leica DC100 microscope with a ×20 objective and a Leica DC100 camera connected to a 2-GHz PC running Leica IM1000 software (Leica GmbH, Wetzlar, Germany). Cell death areas were quantified from immunohistochemistry-stained tumor sections using ImageJ (National Institutes of Health, Bethesda, MD). At higher magnifications (×40), apoptotic cells were counted manually by identifying typical apoptotic bodies. Cell death areas identified had more than 50% of cell death occurring within quantified regions.

Results

Ultrasound data indicated changes in quantitative parameters as noninvasive ultrasound-based biomarkers that could be correlated to the presence of cell death. Figure 1 illustrates representative ultrasound images and histologic data obtained for different times after chemotherapy treatment. Ultrasound results demonstrated increases in backscattered signal intensity and changes in spectral parameters compared to pretreatment data (discussed further below). In general, longer times after treatment typically resulted in larger areas of cell death within the tumor and smaller cell and nucleus sizes, as presented. Figure 2 presents representative parametric maps of the 0-MHz intercept response biomarker overlaid on the corresponding ~7-MHz ultrasound B-mode images for untreated control as well as for different times after treatment. These maps demonstrate the use of a quantitative ultrasound parameter to monitor the treatment response for each individual tumor and can be used to discriminate differences in response between groups of tumors. These maps also demonstrate heterogeneities in the parameters spatially and served as inputs into texture-based analyses.

Specifically, mean increases in the MBF biomarker (MBFΔ) of 0.0 ± 0.1 dB_r, 1.7 ± 0.2 dB_r, 2.4 ± 0.2 dB_r, 6.2 ± 0.3 dB_r, and 7.2 ± 1.3 dB_r were observed for 0, 4, 12, 24, and 48 hours after treatment, respectively. A similar trend was obtained for the 0-MHz interceptΔ biomarker. Results obtained for these spectral parameters have been summarized in Figure 3. As this figure indicates, the data obtained for conventional frequency ultrasound paralleled results observed for high-frequency data for the same treatment groups, respectively.

Spectral slope changes were less prominent and were not shown to be statistically significant (Figure W1).

Results associated with textural parameters are presented in Figure 4 and consist of relative changes in contrast, energy, and homogeneity biomarkers. These were extracted from MBF and 0-MHz intercept parametric maps following the treatment and compared to pretreatment counterparts. Since the resolution of the parametric maps is affected by the axial and lateral resolution in low- and high-frequency ultrasound data that are different, averages of relative changes in the textural parameters were determined to monitor the treatment response. This permitted a direct comparison of the low- and high-frequency data demonstrating similar trends. The results presented in Figure 4 indicate considerable changes in the textural properties of spectral parametric maps for chemotherapy-treated animal-based tumors compared to the untreated control tumors. Whereas the data obtained for conventional frequency ultrasound paralleled results observed for high-frequency data, the high-frequency data demonstrated a greater increase, on average, in the textural parameters extracted from 0-MHz intercept parametric maps. Changes in the textural parameters of MBF parametric maps for high- and conventional frequency data were similar. Results associated with the statistical histogram-based biomarkers demonstrated similar trends, in general, in comparison to those obtained from spectral and textural-based monitoring (Figure W1).

Table 1 outlines the outcomes of tests of significance performed for each response biomarker, using ANOVA test followed by LSD

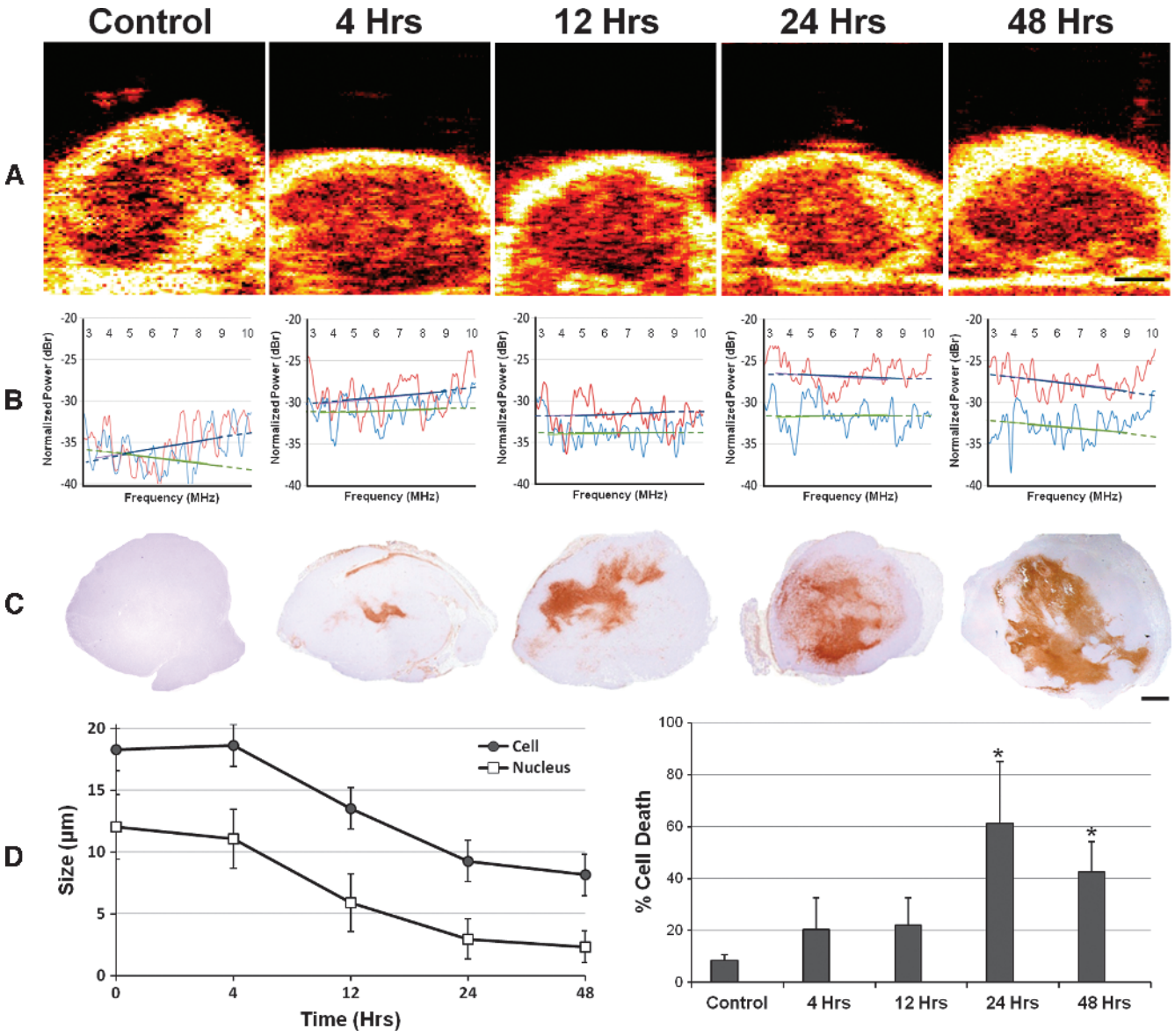

Figure 1. Representative data obtained 0, 4, 12, 24, and 48 hours after treatment. (A) Representative ~7-MHz ultrasound B-mode images of MDA tumors demonstrating increases in tissue echogenicity with treatment in contrast to untreated tumor. The scale bar represents ~3 mm. (B) Representative normalized power spectra obtained from each tumor before treatment and afterward. (C) Low-magnification light microscopy images of ISEL-stained tumors. The scale bar represents ~1 mm. (D) Average cell and nucleus sizes measured for different times after treatment using high-magnification images of H&E-stained tumor slices (left) and mean areas of apoptotic cell death measured for different times after treatment using ISEL staining (right). Error bars represent ±1 SD. Stars represent statistically significant differences ($P < .05$) in comparison to the control.

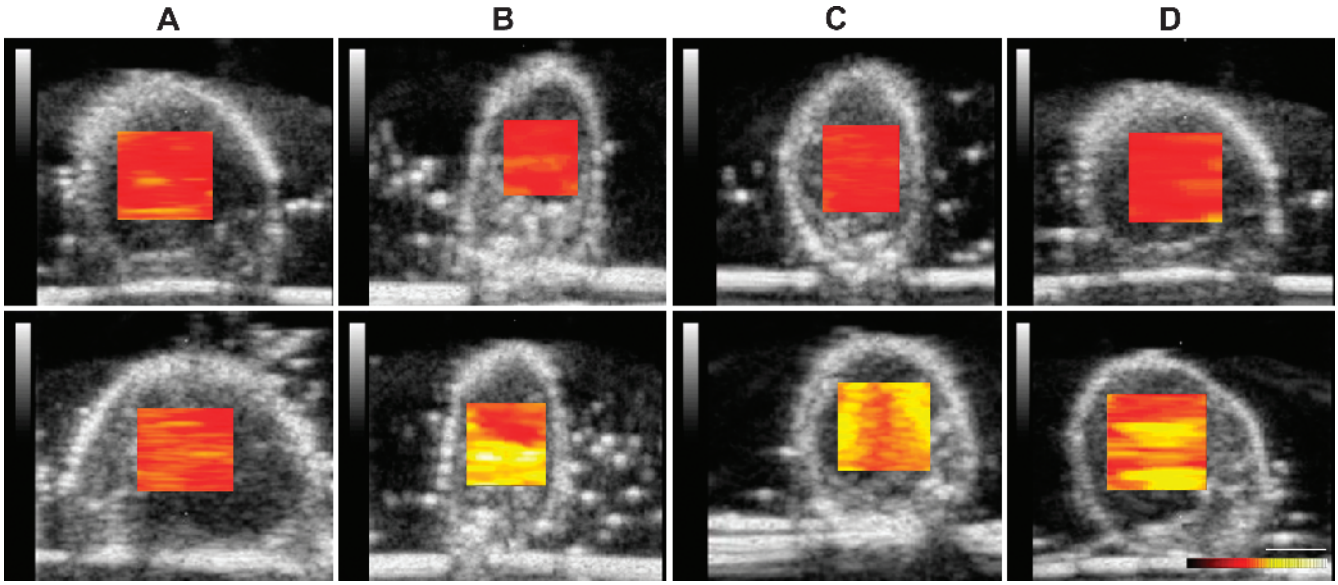

Figure 2. Conventional frequency ultrasound B-mode images with ROI parametric overlays of the 0-MHz intercept biomarker for tumors treated with paclitaxel-doxorubicin and imaged before and after (A) 4, (B) 12, (C) 24, and (D) 48 hours. The top row of images consists of data acquired before treatment, and the bottom row corresponds to those obtained at the specified times after the treatment. Scale bars represent ~5 mm. The color bar represents a scale encompassing ~100 dB_r.

post hoc test for the significant biomarkers. According to the results presented, average changes in the MBF biomarker, as well as in the contrast of its corresponding parametric maps, showed statistically significant differences compared to the untreated control group, after 12 hours of chemotherapy for both conventional and high-frequency data. Statistically significant differences were revealed for the 0-MHz intercept biomarker and its corresponding textural parameters after 12 to 24 hours of therapy for low- and high-frequency data.

Histologic analyses of breast cancer xenograft tumor responses to treatment administration were carried out using light microscopy and image analysis with H&E and ISEL staining to quantify macroscopic regions of cell death tissue response (Figure 1). Staining for cell death revealed 8 ± 2%, 20 ± 12%, 22 ± 10%, 61 ± 24%, and 42 ± 11% mean areas (±SD) of apoptotic cell death in tumor samples 0, 4, 12, 24, and 48 hours after treatment, respectively. Tests of significance indicated that there were statistically significant differences between the amounts of histologic apoptotic cell death beginning 24 hours after treatment compared to the untreated control animals (Table 1).

Linear regression analyses were performed to evaluate correlations between changes in the conventional frequency ultrasound spectral parameters, or the relative changes in the textural properties of the spectral parametric maps, and tumor cell death measurements obtained from histologic analysis. The analysis resulted in r^2 values ranging from 0.60 to 0.94 (Table 1) for single parameters. Multiple regression analysis was also performed to find an optimal linear combination of spectral and textural biomarkers to obtain a more robust hybrid biomarker demonstrating higher levels of correlation with histologic tumor cell death measurements. All parameters were first standardized to obtain random variables with mean of 0 and SD of 1, having a similar potential importance in the model. The parameters

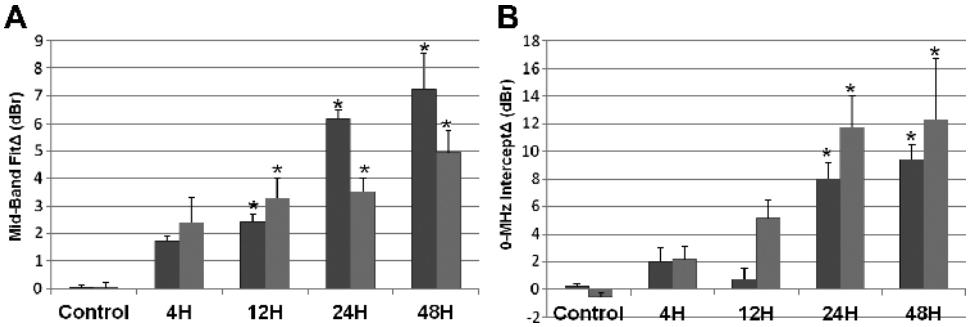

Figure 3. Changes in ultrasound-based spectral biomarkers of treatment response compared to pretreatment. (A) MBFΔ results for conventional and high-frequency data acquired before and at different times after treatment. Control animals are untreated; (B) 0-MHz interceptΔ results for high- and low-frequency data acquired at different times after treatment. Dark and light bars represent conventional low- and high-frequency data, respectively. Error bars represent ±1 SE. Stars represent statistically significant differences ($P < .05$) in comparison to the control.

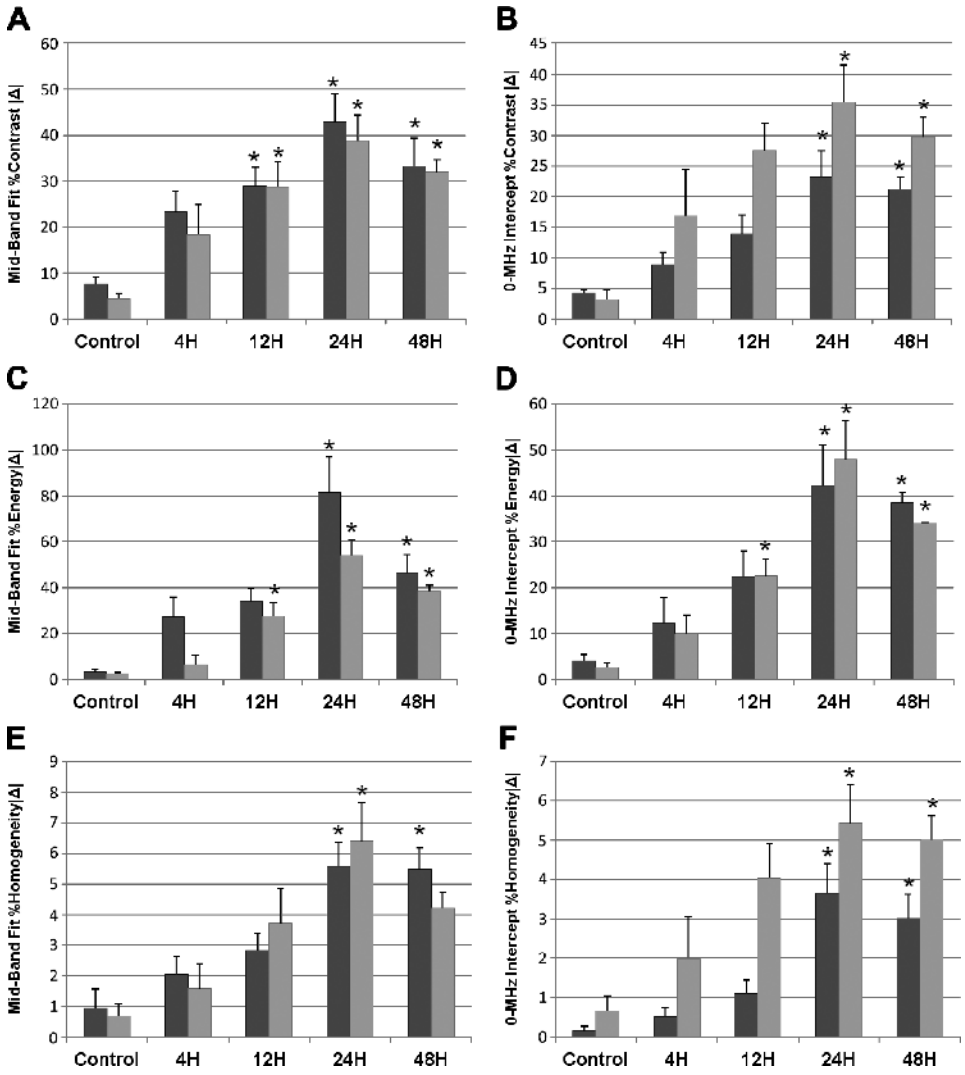

Figure 4. (A–F) Relative changes in ultrasound-based textural biomarkers of treatment response for conventional and high-frequency data acquired before and at different times after treatment. All the relative changes are in percent compared to pretreatment. Control animals are untreated. Dark and light bars represent conventional low- and high-frequency data, respectively. Error bars represent ±1 SE. Stars represent statistically significant differences ($P < .05$) in comparison to the control.

Table 1. Summary of *P* Values Obtained from Statistical Tests of Significance Carried Out for the Histologic Tumor Cell Death Measurements, as well as for Changes in High-Frequency Ultrasound (HFU)– and Conventional Frequency Ultrasound (CFU)–Based Biomarkers Using ANOVA Test over All Treatment Groups, Followed by LSD Post Hoc Test for Each Treated Group *versus* the Untreated Control Group.

	ANOVA Test		LSD Post Hoc Test (*versus* Untreated Control Group)								Correlation with %Cell Death (r^2)
			4 Hours		12 Hours		24 Hours		48 Hours		
Cell Death	0.005**		0.383		0.295		0.001**		0.027*		
	CFU	HFU	CFU	HFU	CFU	HFU	CFU	HFU	CFU	HFU	
MBF	0.000***	0.042*	0.097	0.078	0.017*	0.018*	0.000***	0.015*	0.000***	0.005**	0.67
MBF contrast	0.016*	0.029*	0.107	0.172	0.024*	0.022*	0.001**	0.004**	0.015*	0.029*	0.63
MBF energy	0.003**	0.000***	0.189	0.703	0.076	0.017*	0.000***	0.000***	0.028*	0.006**	0.93
MBF homogeneity	0.004**	0.034*	0.464	0.633	0.182	0.109	0.001**	0.008**	0.009**	0.117	0.92
0-MHz intercept	0.000***	0.003**	0.308	0.394	0.749	0.077	0.000***	0.002**	0.000***	0.003**	0.61
0-MHz intercept contrast	0.016*	0.045*	0.425	0.186	0.091	0.024*	0.004**	0.006**	0.012*	0.036*	0.60
0-MHz intercept energy	0.011*	0.001**	0.474	0.422	0.097	0.039*	0.004**	0.000***	0.009**	0.010*	0.79
0-MHz intercept homogeneity	0.002**	0.037*	0.707	0.404	0.276	0.043	0.001**	0.009**	0.008**	0.031*	0.94

The last column represents the r^2 values obtained from regression analysis performed to evaluate correlations between changes in the conventional frequency quantitative ultrasound-based biomarkers and the histologic tumor cell death estimates.

*Statistically significant ($P < .05$).

**Statistically highly significant ($P < .01$).

***Statistically extremely significant ($P < .001$).

with no significant contribution to the model ($P > .05$) were then eliminated through an iterative backward method. This resulted in a final model only depending on MBF %energyΔ and 0-MHz intercept %homogeneityΔ parameters (Equation 1), correlating to histologic tumor cell death measurements with an r^2 value of 0.97, i.e.,

$$\text{Hybrid biomarker} = 0.46 \times \text{standardized}\{\text{MBF \%energy}\Delta\} + 0.54 \times \text{standardized}\{\text{0-MHz intercept \%homogeneity}\Delta\}(\text{A.U.}) \quad (1)$$

Figure 5 presents fitted lines to the scatter data in conjunction with the 95% confidence intervals for MBFΔ, MBF %energyΔ, 0-MHz interceptΔ, 0-MHz intercept %homogeneityΔ, and the hybrid biomarker, respectively. Regression analysis indicated a strong correlation, particularly, between quantitative ultrasound-based textural biomarkers and histologic tumor cell death responses to treatment.

Discussion and Conclusions

The results presented in this study confirm, for the first time, that quantitative ultrasound techniques at clinically relevant conventional frequencies, in conjunction with textural characterization methods, can be used to monitor noninvasively cell death progress *in vivo*. In comparison with untreated control animals, ultrasound-based spectral biomarkers (MBF and 0-MHz intercept parameters), and textural biomarkers (contrast, energy, and homogeneity parameters extracted from MBF and 0-MHz intercept parametric maps), indicated changes associated with histologic increases in cell death. We have demonstrated the possibility of cell death detection using high-frequency ultrasound

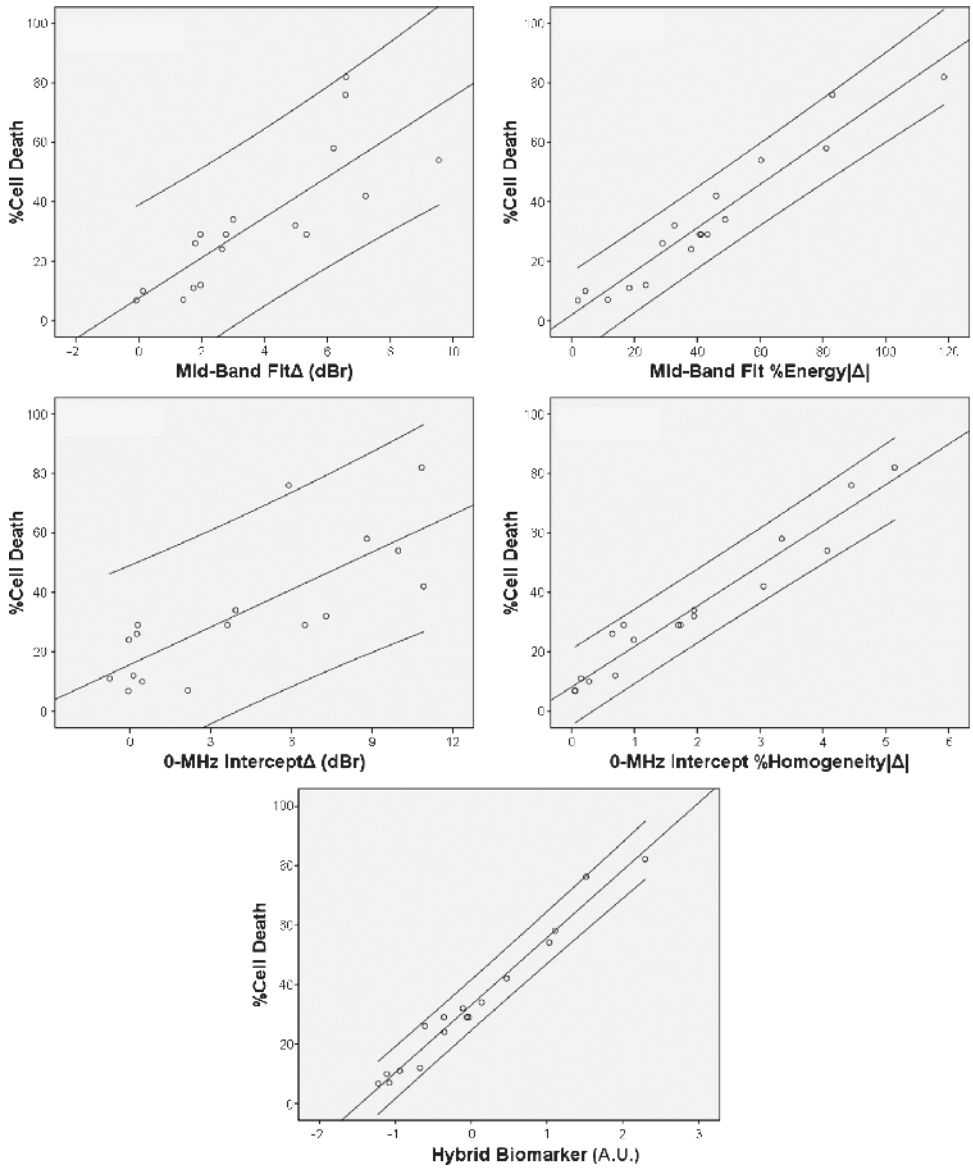

Figure 5. Results of regression analysis performed to evaluate correlations between changes in the conventional frequency quantitative ultrasound-based biomarkers and tumor cell death measurements obtained from histologic analysis. The analysis resulted in an r^2 value of 0.67 (MBFΔ), 0.93 (MBF %energyΔ), 0.61 (0-MHz interceptΔ), 0.94 (0-MHz intercept %homogeneityΔ), and 0.97 (hybrid biomarker) from left to right and top to bottom, respectively.

previously [12–14]. Here, we demonstrate these methods coupled with textural analysis in a clinically relevant ultrasound frequency range.

Changes in mean spectral parameters, as well as in textural patterns of spectral parametric maps corresponding at different times after chemotherapy administration, were detectable. Particularly in samples demonstrating macroscopic areas of cell death, increased backscattered signal intensity in the low- and high-frequency ultrasound images was observed. Backscattered signal intensity increased for samples of different tumor groups assessed at different times after chemotherapy treatment. This was concordant with increases in cell death apparent histologically. Data indicated that ~20% cell death in an ~1-cm xenograft tumor was detectable after 12 to 24 hours of chemotherapy administration with statistical significance, in well-controlled animal tumor models. This indicated a reasonable sensitivity of the conventional frequency quantitative ultrasound techniques to detect noninvasively early cell death changes in tumors.

Linear regression analysis performed demonstrated strong correlations between changes in determined ultrasound-based biomarkers with tumor cell death measurements obtained from histologic analysis. Although single spectral biomarkers demonstrated a favorable correlation with the amount of histologic cell death (with maximum r^2 = 0.67, $P < .001$), textural biomarkers exhibited an even stronger correlation (with maximum r^2 = 0.94, $P < .001$). This suggests strong potential for using the higher order information extracted from ultrasonic spectral parametric maps, instead of using a simple averaging, to better estimate levels of cell death, noninvasively.

The determined spectral and textural biomarkers indicated similar changes in trend for high- and low-frequency ultrasound data. This is in line with the results of previous studies where it has been demonstrated that nuclear morphology influences scattering at high and lower ultrasound frequencies [13,15]. Confirmatory changes in statistical parameters of the signal envelope were also observed with cell death, for both high and conventional frequency ultrasound data. These measures have been applied before using high-frequency ultrasound for cells treated with chemotherapy [11].

Previous investigations of ultrasonic cell death detection *in vitro* and *in vivo* support the results presented in this study. Previous studies include those investigations where apoptosis was induced in cells and normal tissues using a variety of modalities and analyzed using high-frequency ultrasound [8–15]. Those studies also indicated an important role of nuclear structure in the detection of cell death. In particular, it was demonstrated that nuclear condensation caused by the induction of apoptotic death can lead to increases in backscattered signal intensity. This is consistent with observations in this study using high- and now low-frequency ultrasound. In addition, comparative studies performed previously on low- and high-frequency ultrasound data from *in vitro* cell models indicated a correspondence consistent with that seen here [39]. Here, we followed cell death progression with time and thus monitored the extent of cell death ultrasonically.

Samples imaged in this study using conventional frequency ultrasound demonstrated that increases in cell death had consequent changes in spectral, textural, and statistical parameters. All such increases followed the trends of increases in cell death in tumors as obtained from histologic analyses. The fact the low-frequency data were parallel in trend by the high-frequency data was confirmatory. This is despite the fact that different scattering modes were potentially expected from these two frequency ranges. It is expected that more Faran-like scattering [40] would be observed with high-frequency ultrasound since cellular components are approximately proportional to these wavelengths. In contrast, at low frequencies, Rayleigh scattering [41] is anticipated to be predominant as the cellular components are considerably smaller than the ultrasound wavelengths. The observation that both ultrasound ranges are sensitive to cell death is not necessarily surprising given that ultrasound interacts with cell ensembles in both cases and nuclear structure in those ensembles changes with cell death. There are also cellular changes in viscosity and elasticity, as well as density associated with cell death [13]. Increases observed in ultrasound backscattered signal intensity can be mainly linked to the condensation of nuclear structure during apoptosis and cell death (pyknosis and karyorrhexis). There is now extensive experimental evidence suggesting a role for nuclear structure in contributing to ultrasound backscattered signals [13]. This evidence includes the following:

1. In highly cellular xenograft tumors, backscattered signals and spectra are identical to backscattered signals and spectra of centrifuged cell models that mimic the histologic packing of xenograft tumors [42]. Such packed cell models have no extracellular matrix and collagen present yet exhibit nearly identical backscatter profiles.
2. Different cell types may be differentiated on the basis of their ultrasound spectra, now recognized to be linked to nuclear size [15].
3. Calculated scatterer sizes from ultrasound backscattered signal do not work out to be the same as cell sizes but coincide with smaller sizes near that of nuclei, which again suggests an important role of the nucleus [42].

It might be argued that measurable changes in backscatter characteristics from micron-sized particles are not expected at low frequencies, mainly due to loss of scattering strength of small scattering structures. However, in the low- to mid-frequency range (near 10 MHz), bulk changes in tissue are mostly related to ensembles of cells and nuclei smaller than the wavelength of the ultrasound being used. Such ensembles influence acoustic properties and thus ultrasound backscatter characteristics [43]. When imaging cell samples, even at these low frequencies, a speckle pattern is still formed indicating that many subresolution scatterers contribute to detected signals [39]. Similar conclusions can be made considering backscattered signal intensity from tumor samples.

The textural parameters in this study based on spatial maps of quantitative ultrasound spectral parameters were more sensitive to cell death than averaged spectral parameters. They were able to detect changes in tissue microstructures with a higher correlation to histologic cell death. This is likely due to the fact that the tumor responses, as observed in this study in xenografts, are heterogeneous (Figure 1) and not homogeneous. Thus, an analysis that takes those features into account is, in particular, advantageous. Here, we studied responses of tumors to chemotherapy, but the same method can be applied in the situations where heterogeneous responses occur. This can happen in radiation treatments [14], or even with photodynamic therapy [9,13], or new vascular disrupting treatments [44].

The technique introduced in this work complements other imaging methods, e.g., magnetic resonance imaging or positron emission tomography, proposed to detect tumor responses [5,45,46]. Unlike these methods, the quantitative ultrasound method relies on inherent contrast changes arising from changes in acoustical properties as cancer cells die. In addition, the preclinical work here applied in xenograft models appears to be adaptable to human data for response

monitoring [43,47] and may complement clinical methods (above) for therapy response monitoring.

In conclusion, this study suggests that quantitative conventional frequency ultrasound in conjunction with the textural analysis techniques may be used to monitor cell death *in vivo*. Data were obtained in a timeline basis, for five different times after chemotherapy in preclinical breast cancer xenografts. Analyses indicated favorable correlations between changes in ultrasonic quantitative biomarkers of treatment response and the histologic extent of cell death, particularly when textural characteristics of spectral parametric maps were applied. This work forms the basis for the application of clinically relevant conventional frequency approaches *in vivo* in cancer patients for monitoring and personalization of their cancer therapies. This is a clinical application of the proposed method where the process to be monitored generates the contrast by itself.

References

[1] Huang E, McNeese MD, Strom EA, Perkins GH, Katz A, Hortobagyi GN, Valero V, Kuerer HM, Singletary SE, Hunt KK, et al. (2002). Locoregional treatment outcomes for inoperable anthracycline-resistant breast cancer. *Int J Radiat Oncol Biol Phys* **53**, 1225–1233.

[2] Fisher B, Bryant J, Wolmark N, Mamounas E, Brown A, Fisher ER, Wickerham DL, Begovic M, DeCillis A, Robidoux A, et al. (1998). Effect of preoperative chemotherapy on the outcome of women with operable breast cancer. *J Clin Oncol* **16**, 2672–2685.

[3] Smith IC, Heys SD, Hutcheon AW, Miller ID, Payne S, Gilbert FJ, Ah-See AK, Eremin O, Walker LG, Sarkar TK, et al. (2002). Neoadjuvant chemotherapy in breast cancer: significantly enhanced response with docetaxel. *J Clin Oncol* **20**, 1456–1466.

[4] Chollet P, Charrier S, Brain E, Curé H, van Praagh I, Feillel V, de Latour M, Dauplat J, Misset JL, and Ferrière JP (1997). Clinical and pathological response to primary chemotherapy in operable breast cancer. *Eur J Cancer* **33**, 862–866.

[5] Brindle K (2008). New approaches for imaging tumour responses to treatment. *Nat Rev Cancer* **8**, 94–107.

[6] Sadeghi-Naini A, Falou O, Hudson JM, Bailey C, Burns PN, Yaffe MJ, Stanisz GJ, Kolios MC, and Czarnota GJ (2012). Imaging innovations for cancer therapy response monitoring. *Imaging Med* **4**, 311–327.

[7] Falou O, Soliman H, Sadeghi-Naini A, Iradji S, Lemon-Wong S, Zubovits J, Spayne J, Dent R, Trudeau M, Boileau JF, et al. (2012). Diffuse optical spectroscopy evaluation of treatment response in women with locally advanced breast cancer receiving neoadjuvant chemotherapy. *Transl Oncol* **5**, 238–246.

[8] Czarnota GJ, Kolios MC, Vaziri H, Benchimol S, Ottensmeyer FP, Sherar MD, and Hunt JW (1997). Ultrasonic biomicroscopy of viable, dead and apoptotic cells. *Ultrasound Med Biol* **23**, 961–965.

[9] Czarnota GJ, Kolios MC, Abraham J, Portnoy M, Ottensmeyer FP, Hunt JW, and Sherar MD (1999). Ultrasound imaging of apoptosis: high-resolution non-invasive monitoring of programmed cell death *in vitro*, *in situ* and *in vivo*. *Br J Cancer* **81**, 520–527.

[10] Kolios MC, Czarnota GJ, Hussain M, Foster FS, Hunt JW, and Sherar MD (2001). Analysis of ultrasound backscatter from ensembles of cells and isolated nuclei. In *Proceedings of IEEE Ultrasonics Symposium, Orlando, FL,* **Vol 2**, pp. 1257–1260.

[11] Tunis AS, Czarnota GJ, Giles A, Sherar MD, Hunt JW, and Kolios MC (2005). Monitoring structural changes in cells with high-frequency ultrasound signal statistics. *Ultrasound Med Biol* **31**, 1041–1049.

[12] Vlad RM, Alajez NM, Giles A, Kolios MC, and Czarnota GJ (2008). Quantitative ultrasound characterization of cancer radiotherapy effects *in vitro*. *Int J Radiat Oncol Biol Phys* **72**, 1236–1243.

[13] Banihashemi B, Vlad R, Debeljevic B, Giles A, Kolios MC, and Czarnota GJ (2008). Ultrasound imaging of apoptosis in tumor response: novel preclinical monitoring of photodynamic therapy effects. *Cancer Res* **68**, 8590–8596.

[14] Vlad RM, Brand S, Giles A, Kolios MC, and Czarnota GJ (2009). Quantitative ultrasound characterization of responses to radiotherapy in cancer mouse models. *Clin Cancer Res* **15**, 2067–2075.

[15] Taggart LR, Baddour RE, Giles A, Czarnota GJ, and Kolios MC (2007). Ultrasonic characterization of whole cells and isolated nuclei. *Ultrasound Med Biol* **33**, 389–401.

[16] Guimond A, Teletin M, Garo E, D'Sa A, Selloum M, Champy M-F, Vonesch J-L, and Monassier L (2007). Quantitative ultrasonic tissue characterization as a new tool for continuous monitoring of chronic liver remodelling in mice. *Liver Int* **27**, 854–864.

[17] Feleppa EJ, Kalisz A, Sokil-melgar JB, Lizzi FL, Liu T, Rosado AL, Shao MC, Fair WR, Wang Y, Cookson MS, et al. (1996). Typing of prostate tissue by ultrasonic spectrum analysis. *IEEE Trans Ultrason Ferroelectr Freq Control* **43**, 609–619.

[18] Yang M, Krueger TM, Miller JG, and Holland MR (2007). Characterization of anisotropic myocardial backscatter using spectral slope, intercept and midband fit parameters. *Ultrason Imaging* **29**, 122–134.

[19] Oelze ML, O'Brien WD, Blue JP, and Zachary JF (2004). Differentiation and characterization of rat mammary fibroadenomas and 4T1 mouse carcinomas using quantitative ultrasound imaging. *IEEE Trans Med Imaging* **23**, 764–771.

[20] Feleppa EJ, Mamou J, Porter CR, and Machi J (2011). Quantitative ultrasound in cancer imaging. *Semin Oncol* **38**, 136–150.

[21] Ignee A, Jedrejczyk M, Schuessler G, Jakubowski W, and Dietrich CF (2010). Quantitative contrast enhanced ultrasound of the liver for time intensity curves—reliability and potential sources of errors. *Eur J Radiol* **73**, 153–158.

[22] Zagzebski JA, Lu ZF, and Yao LX (1993). Quantitative ultrasound imaging: *in vivo* results in normal liver. *Ultrason Imaging* **15**, 335–351.

[23] Ziegler LE, O'Brien RT, Waller KR, and Zagzebski JA (2003). Quantitative contrast harmonic ultrasound imaging of normal canine liver. *Vet Radiol Ultrasound* **44**, 451–454.

[24] Pluskiewicz W, Zywiec J, Zwiec J, Gumprecht J, and Grzeszczak W (2007). Quantitative ultrasound of phalanges of adults with end-stage renal disease or who have undergone renal transplantation. *Ultrasound Med Biol* **33**, 1353–1361.

[25] Wong IY-Z, Copp HL, Clark CJ, Wu H-Y, and Shortliffe LD (2009). Quantitative ultrasound renal parenchymal area correlates with renal volume and identifies reflux nephropathy. *J Urol* **182**, 1683–1687.

[26] Gerst S, Hann LE, Li D, Gonen M, Tickoo S, Sohn MJ, and Russo P (2011). Evaluation of renal masses with contrast-enhanced ultrasound: initial experience. *AJR Am J Roentgenol* **197**, 897–906.

[27] Liao Y-Y, Tsui P-H, Li C-H, Chang K-J, Kuo W-H, Chang C-C, and Yeh C-K (2011). Classification of scattering media within benign and malignant breast tumors based on ultrasound texture-feature-based and Nakagami-parameter images. *Med Phys* **38**, 2198–2207.

[28] Hashimoto H, Suzuki M, Oshida M, Nagashima T, Yagata H, Shishikura T, Imanaka N, and Nakajima N (2000). Quantitative ultrasound as a predictor of node metastases and prognosis in patients with breast cancer. *Breast Cancer* **7**, 241–246.

[29] Sadigh G, Carlos RC, Neal CH, and Dwamena BA (2012). Accuracy of quantitative ultrasound elastography for differentiation of malignant and benign breast abnormalities: a meta-analysis. *Breast Cancer Res Treat* **134**, 923–931.

[30] Lizzi FL, Ostromogilsky M, Feleppa EJ, Rorke MC, and Yaremko MM (1987). Relationship of ultrasonic spectral parameters to features of tissue microstructure. *IEEE Trans Ultrason Ferroelectr Freq Control* **34**, 319–329.

[31] Lizzi FL, Astor M, Liu T, Deng C, Coleman DJ, and Silverman RH (1997). Ultrasonic spectrum analysis for tissue assays and therapy evaluation. *Int J Imaging Syst Technol* **8**, 3–10.

[32] Lizzi FL, Greenebaum M, Feleppa EJ, Elbaum M, and Coleman DJ (1983). Theoretical framework for spectrum analysis in ultrasonic tissue characterization. *J Acoust Soc Am* **73**, 1366–1373.

[33] Haralick RM, Shanmugam K, and Dinstein I (1973). Textural features for image classification. *IEEE Trans Syst Man Cybern A Syst Hum* **3**, 610–621.

[34] Molthen RC, Shankar PM, Reid JM, Forsberg F, Halpern EJ, Piccoli CW, and Goldberg BB (1998). Comparisons of the Rayleigh and K-distribution models using *in vivo* breast and liver tissue. *Ultrasound Med Biol* **24**, 93–100.

[35] Dong F, Madsen EL, MacDonald MC, and Zagzebski JA (1999). Nonlinearity parameter for tissue-mimicking materials. *Ultrasound Med Biol* **25**, 831–838.

[36] Feleppa EJ, Lizzi FL, Coleman DJ, and Yaremko MM (1986). Diagnostic spectrum analysis in ophthalmology: a physical perspective. *Ultrasound Med Biol* **12**, 623–631.

[37] Oelze ML and O'Brien WD (2002). Method of improved scatterer size estimation and application to parametric imaging using ultrasound. *J Acoust Soc Am* **112**, 3053–3063.

[38] Scott DW (1979). On optimal and data-based histograms. *Biometrika* **66**, 605–610.

[39] Azrif M, Ranieri S, Giles A, Debeljevic B, Kolios MC, and Czarnota GJ (2007). Conventional low-frequency ultrasound detection of apoptosis. In *Proceedings of American Institute of Ultrasound in Medicine Annual Convention, New York, NY,* p. S185.

[40] Faran JJ (1951). Sound scattering by solid cylinders and spheres. *J Acoust Soc Am* **23**, 405.

[41] Strutt JW (1871). Investigation of the disturbance produced by a spherical obstacle on the waves of sound. *Proc Lond Math Soc* **s1–4**, 253–283.

[42] Oelze ML and O'Brien WD (2006). Application of three scattering models to characterization of solid tumors in mice. *Ultrason Imaging* **28**, 83–96.

[43] Sadeghi-Naini A, Falou O, and Czarnota GJ (2012). Quantitative ultrasound visualization of cell death: emerging clinical applications for detection of cancer treatment response. In *Proceedings of 34th Annual International Conference of the IEEE Engineering in Medicine and Biology Society (EMBC), San Diego, CA,* pp. 1125–1128.

[44] Czarnota GJ, Karshafian R, Burns PN, Wong S, Al Mahrouki A, Lee JW, Caissie A, Tran W, Kim C, Furukawa M, et al. (2012). Tumor radiation response enhancement by acoustical stimulation of the vasculature. *Proc Natl Acad Sci USA* **109**, E2033–E2041.

[45] Witney TH and Brindle KM (2010). Imaging tumour cell metabolism using hyperpolarized ^{13}C magnetic resonance spectroscopy. *Biochem Soc Trans* **38**, 1220–1224.

[46] Witney TH, Kettunen MI, Hu D, Gallagher FA, Bohndiek SE, Napolitano R, and Brindle KM (2010). Detecting treatment response in a model of human breast adenocarcinoma using hyperpolarised [1-^{13}C]pyruvate and [1,4-$^{13}C_2$] fumarate. *Br J Cancer* **103**, 1400–1406.

[47] Sadeghi-Naini A, Falou O, and Czarnota GJ (2012). Quantitative ultrasound spectral parametric maps: early surrogates of cancer treatment response. In *Proceedings of 34th Annual International Conference of the IEEE Engineering in Medicine and Biology Society (EMBC), San Diego, CA,* pp. 2672–2675.

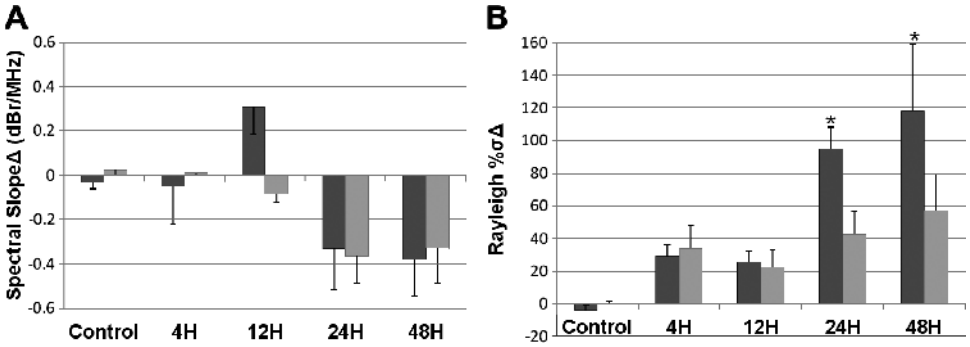

Figure W1. (A) Changes in spectral slope biomarker (Spectral SlopeΔ), and (B) relative changes in ultrasound-based statistical biomarker of treatment response (Rayleigh %σΔ), for conventional and high-frequency data acquired before and at different times after treatment. The relative changes are in percent compared to pretreatment. Control animals are untreated. Dark and light bars represent conventional low- and high-frequency data, respectively. Error bars represent ±1 SE. Stars represent statistically significant differences ($P < .05$) in comparison to the control.